# Degradation of polymetallic nodules during hydraulic transport under influence of particle-wall and particle-particle interaction

de Hoog, E.; van Wijk, J. M.; Wijnands, J. T.M.; Talmon, A. M.

**DOI**
10.1016/j.mineng.2020.106415

**Publication date**
2020

**Document Version**
Final published version

**Published in**
Minerals Engineering

**Citation (APA)**
de Hoog, E., van Wijk, J. M., Wijnands, J. T. M., & Talmon, A. M. (2020). Degradation of polymetallic nodules during hydraulic transport under influence of particle-wall and particle-particle interaction. *Minerals Engineering*, *155*, Article 106415. https://doi.org/10.1016/j.mineng.2020.106415

Minerals Engineering 155 (2020) 106415

Contents lists available at ScienceDirect

Minerals Engineering

journal homepage: www.elsevier.com/locate/mineng

# Degradation of polymetallic nodules during hydraulic transport under influence of particle-wall and particle-particle interaction

E. de Hoog[a,b], J.M. van Wijk[a,*], J.T.M. Wijnands[a], A.M. Talmon[c,b]

[a] Royal IHC, the Netherlands
[b] Delft University of Technology, the Netherlands
[c] Deltares, the Netherlands

ARTICLE INFO

*Keywords:*
Particle wear
Abrasion
Attrition
Polymetallic nodules
Vertical transport
Manganese nodules
Wear experiments
Deep ocean mining

ABSTRACT

The mining of polymetallic nodules from the seafloor at depths down to 6000 m requires the excavation of nodules with a seafloor mining tool, the transport of nodules as a slurry through a jumper hose connecting the mining tool to a vertical hydraulic transport system and the transport of the nodules through the vertical lifting pipe. We focus on a concept with conventional hydraulic transport, using a series of centrifugal pump booster stations. The nodules will be transported in different flow regimes, ranging from a sliding bed (in the jumper hose) to a homogeneous suspension (vertical flow). Each regime gives rise to degradation of the nodules in a different way. It is important to understand the degradation mechanisms in detail in order to predict the particle size distribution of the slurry leaving the riser. This particle size distribution is a key design parameter for design of processing equipment and for environmental impact assessment. In this article we present the results of experimental work on abrasive wear (particle-wall interaction) and attrition (particle-particle interaction) of polymetallic nodules from the Clarion Clipperton Zone and we discuss its applicability to engineering practice.

## 1. Introduction

The mining of polymetallic nodules from the seafloor at depths down to about 6000 m requires the excavation of nodules with a seafloor mining tool (SMT), the transport of nodules as a slurry through a jumper hose connecting the mining tool to the vertical hydraulic transport system (VTS) and the transport of the nodules through the riser. We focus on a concept with conventional hydraulic transport, using a series of centrifugal pump booster stations, see Fig. 1. In this concept pre-sizing of the nodules is not necessary and any size reduction could be attributed to degradation induced by interaction with pumps, pipelines and other nodules. The particle size distribution (PSD) of the mixture leaving the riser is an important design parameter for the processing equipment and it is an important parameter for environmental impact assessment in case of return flow of sediments to the seafloor. Especially the fraction of fine material (smaller than 63 μm) is of interest. Currently there is no data of the degradation of polymetallic nodules by abrasion and attrition to allow for calculation of the PSD's after the transport process. This work aims to provide an experimental methodology of which the results can be used for engineering purposes. This is achieved by investigating the extremes of degradation encountered in various parts of the transport system, thus to create a bandwidth of possible degradation rates and a conservative estimate of nodule degradation under operational conditions.

Particle degradation occurs in all multiphase flows involving solids in a carrier fluid. Depending on the force magnitude and direction, the modes of degradation can be identified as attrition, fragmentation, abrasion and chipping (Van Laarhoven, 2010). The degradation process is closely linked to the hydraulic transport process and the associated components. The centrifugal pump will provide high impact forces in normal direction, causing impact fragmentation. This specific topic has been extensively reported in Van Wijk et al. (2019), where the impact fragmentation of nodules from the Clarion Clipperton Zone (CCZ) under deep ocean pressure conditions was investigated. In this article this line of research is continued, now focusing on the attrition, chipping and abrasion of similar CCZ nodules under different flow conditions. Van Wijk et al. (2019) showed that the deep ocean pressure conditions have no significant influence on the impact fragmentation process. Since

* Corresponding author.
*E-mail addresses:* e.dehoog@royalihc.com (E. de Hoog), jm.vanwijk@royalihc.com (J.M. van Wijk), j.wijnands@royalihc.com (J.T.M. Wijnands), a.m.talmon@tudelft.nl (A.M. Talmon).
*URLs:* http://www.royalihc.com, http://www.tudelft.nl (E. de Hoog), http://www.royalihc.com (J.M. van Wijk), http://www.royalihc.com (J.T.M. Wijnands), http://www.deltares.nl, http://www.tudelft.nl (A.M. Talmon).

https://doi.org/10.1016/j.mineng.2020.106415
Received 20 August 2019; Received in revised form 23 April 2020; Accepted 30 April 2020

**Nomenclature**

| | |
|---|---|
| $c_v$ | Volume fraction of solids in a mixture [–] |
| $C_D$ | Particle drag coefficient [–] |
| $d$ | Particle diameter [mm] |
| $d_m$ | Mean particle diameter [mm] |
| $D$ | Pipeline (inner) diameter [m] |
| $F_n$ | Normal force [N] |
| $g$ | Gravitational acceleration [m/s$^2$] |
| $k$ | Specific wear rate (Archard) [mm$^2$/N] |
| $m$ | Mass [kg] |
| $m_0$ | Initial mass [kg] |
| $m_1$ | Post-experiment mass [kg] |
| $n$ | Hindered settling exponent [–] |
| $P$ | Rouse number [–] |
| $Re_p$ | Particle Reynolds number [–] |
| $s$ | Sliding distance [m] |
| $St$ | Stokes number [–] |
| $t$ | Time [s] |
| $t_f$ | Reaction time fluid field [s] |
| $t_p$ | Reaction time particle [s] |
| $v_f$ | Fluid velocity [m/s] |
| $v_m$ | Mixture velocity [m/s] |
| $v_s$ | Solids velocity [m/s] |
| $v_{sl}$ | Relative velocity solids-mixture [m/s] |
| $V$ | Worn volume [m$^3$] |
| $w_t$ | Particle terminal settling velocity [m/s] |
| $\rho_d$ | Nodule submerged density [kg/m$^3$] |
| $\rho_f$ | Fluid density [kg/m$^3$] |
| $\rho_s$ | Solids density [kg/m$^3$] |
| $\theta$ | Inclination of tilting tube [°] |

*Abbreviations*

| | |
|---|---|
| *CCZ* | Clarion Clipperton Zone |
| *PSD* | Particle Size Distribution |
| *SMT* | Seafloor Mining Tool |
| *VTS* | Vertical Transport System |

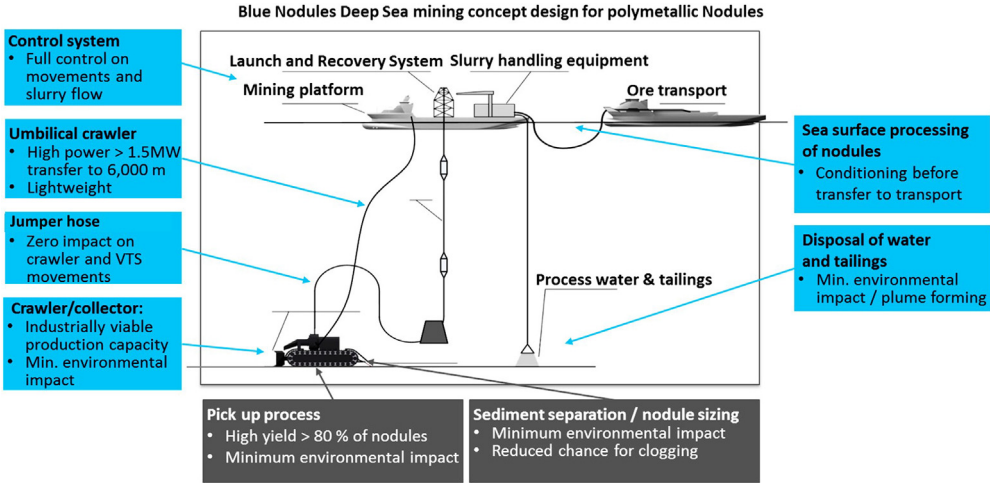


**Fig. 1.** Visual concept of a deep sea mining system. Source: http://www.b.lue-nodules.eu.

attrition, chipping and abrasion are slower processes than impact fragmentation, it is assumed that experiments under atmospheric pressure conditions are representative for the degradation processes.

Following the slurry through the transport system, it first enters the SMT centrifugal pump, where it is subjected to mainly impact fragmentation which is associated with high forces in the normal direction. After that the slurry enters the jumper hose. The lazy-wave configuration of the jumper (Fig. 1) will mainly result in stratification of the slurry, with a sliding bed of nodules and sediments in the inclined and horizontal parts, above which a shear layer will develop. See for instance Vlasak et al. (2013), Ravelet et al. (2013), De Hoog et al. (2017) dealing with coarse particle slurries in horizontal and inclined pipes. The relation between particle degradation and horizontal hydraulic transport has been studied for the transport of coal. Worster and Denny (1955) made an important contribution by relating the degradation of coal to the velocity and transport distance of the coal. Worster and Denny (1955) studied stratified flow regimes, i.e. they encountered a sliding bed with saltation of coal lumps on top of it. Degradation in their work thus is a result from the combined effect of abrasive wear of the coal in the bed layer and attrition of the coal by the higher impacts from the saltating coal in the shear layer (particle-particle interaction).

Continuing with following the slurry, the jumper leads the slurry into the VTS. In the vertical riser two mechanisms dominate the degradation process (Van Wijk, 2016). The first is particle abrasion by particles sliding along the riser segments, which will mainly be the case for the nodules close to the wall. The second mechanism is degradation by particle-particle interaction in the riser segments. Different particle fractions with different sizes have different transport velocities and their relative velocities give rise to collisions and probably mild impact fragmentation, chipping and attrition. Particle-wall interaction will have velocities in the order of the mixture bulk velocity (several meters per second) in the axial direction, resulting in sliding contact. Radial particle velocities will be very limited. Particle-particle interaction will have velocities in the order of the hindered settling velocity (typically between 0–1 m/s for polymetallic nodules of tens of millimeters size), which is an order of magnitude smaller than the bulk velocity.

Proper quantification of the PSD of the slurry leaving the riser requires detailed knowledge on all of the above processes combined with knowledge on the exact behavior of polymetallic nodules under the different flow conditions. The main focus of this article is the abrasion of CCZ polymetallic nodules, with a sidestep to attrition and chipping. The CCZ is of interest for commercial mining and although there is some data on the mechanical properties of polymetallic nodules (Dreiseitl, 2017), there is no research or data known to the authors on either abrasion or attrition of polymetallic nodules.

## 2. Materials and methods

### 2.1. Rationale of the experimental program

To fully understand the wear process of a polymetallic nodule three types of experiments were conducted with polymetallic nodules collected from the GSR license area in the Clarion Clipperton Zone (CCZ). A sample of 100 kg polymetallic CCZ nodules was available for this research. The average density was measured to be $\rho_s = 2497\ \mathrm{kg/m^3}$ with a submerged density of $\rho_d = 1677\ \mathrm{kg/m^3}$ and a 54.8% porosity. A polymetallic nodule is formed as various minerals precipitate from the surrounding water on a nucleus; typically an older nodule, shark tooth, volcanic rock or shell. As the nodule grows a layered internal structure is formed, commonly with local sediments trapped between the layers. These sediments compromise the strength of the nodule and breakages typically occur along these weak points. Larger nodules consist of more layers and weak points, therefore they are usually weaker than smaller nodules as is evident by compressive strength tests by Dreiseitl (2017). Some nodules are an agglomeration of smaller nodules which grew together over time. To keep the geotechnical properties of the nodules sample as close to in situ conditions as possible, the nodules are kept saturated at all time. When nodules are dried their strength decreases as internal sediment (clay) layers dry out and lose their cohesive properties.

The work of Archard (1953) provides the fundamentals of abrasive wear of sliding surfaces. Abrasion takes place due to interaction between the asperities on the sliding surfaces and the effective contact area is dominated by the plastic deformation as a result of the normal load on the surfaces. Archard's work has proven to be valid for abrasive wear predictions for a wide variety of materials, as long as plastic deformation of the surfaces dominate the process. Polymetallic nodules are agglomerates of minerals, being very brittle. The contact interface between a nodule and the pipeline is expected to be highly influenced by the brittle nature of the nodules, so the assumption of pure plastic deformation might only be valid for small contact forces. Moore and King (1980) studied the abrasive wear of brittle solids. In this case the wear is dictated by an interplay between plastic deformation and brittle fracture of the solids. Consequently, the volume of removed material could vary a lot depending on the relative hardness of the materials. In this work Archard (1953) is used as a starting point to study abrasive wear against experimental data.

While Archard (1953) states that the worn volume is proportional to the normal force and the sliding distance, thus being independent of the sliding velocity, Worster and Denny (1955) reported that the worn volume is proportional to $v_m^3 \cdot s^{\frac{1}{2}}$, with $v_m$ the mixture velocity and $s$ the traveled distance. This was measured in a closed loop pipeline circuit where particles collide with bends, pumps and each other. In their case the wear is not solely attributed to abrasion as impacts have played a role as well, possibly explaining the relevance of velocity.

Our first experiment is designed to investigate to what extent the wear of a sliding nodule can be approximated by pure abrasion. In a horizontally orientated setup, without flow, a single nodule slides continuously back and forth. The wear of a single sliding nodule will be studied and the wear equation of Archard (1953) is used to check the velocity-independence-of-worn-volume hypothesis. As put forward earlier, this is not trivial due to the nature of the nodules, i.e. being brittle agglomerates. A single sliding polymetallic nodule gives the easiest conditions to control in the experiment and therefore is a good method to understand the wear process. The largest uncertainties are in the nodules itself, since every nodule differs and mechanical properties of nodules are prone to large statistical deviations (Dreiseitl, 2017). Tests with single nodules will give insight in the magnitude of these deviations and their significance on measuring the wear rate. Additionally, when successful, determining an Archard specific wear rate $k$ allows for quantitative modeling of wear.

In our second set of experiments the wear of a batch of polymetallic nodules is studied. This is to emulate a more realistic wear scenario expected in the lazy-wave configured jumper hose and other horizontal pipes. The transport mode (or flow regime) is expected to have a strong influence on degradation rates, as it is easy to imagine that particles suspended by turbulence will degrade significantly less than particles transported as a saltating sliding bed. A sliding bed flow occurs when the particle diameter $d$ is large relative to the pipe diameter $D$. A rule of thumb for quartz gravels is $d/D > 0.015$ (Wilson et al., 2006), but since polymetallic nodules have a lower density than quartz-based sediments this heuristic is invalid and we consider the Rouse number to judge whether transport is suspended or as bed-load. The Rouse number $P$ is defined as:

$$P = \frac{w_t}{\kappa}\sqrt{\frac{\rho_f}{\tau_b}} \tag{1}$$

With $w_t$ the terminal settling velocity of a nodule, $\kappa$ the von Karman constant, $\rho_f$ the fluid density and $\tau_b$ the bed shear stress (depending on the bed roughness, which is related to the sizes of nodules in the bed). A $P > 2.5$ suggests saltating transport with frequent particle collisions. For sliding bed flow in pipelines the Rouse number can be estimated from the bed shear stress caused by the velocity difference between the sliding bed and the shear flow. The bed shear stress can be estimated using the equivalent hydraulic roughness principle Wilson et al. (2006). Typical conditions in a jumper hose are, $d_{50} = 35$ mm, $D = 0.3$ m$j$, $\rho_d = 1677\ \mathrm{kg/m^3}$ (the submerged density of the nodule) and $v_m = 5.5$ m/s. This results in $4 < P < 5$ depending on the concentration in the pipeline, showing the transport mode is indeed a sliding bed with saltation. The experiment should emulate this.

Where the first two experiments are designed to isolate the individual degradation processes of pure abrasion and the combined abrasion and chipping by saltating transport in a sliding bed, the third experiment is designed to study particle-particle interaction in the VTS. Since long distance vertical transport tests are not possible in a laboratory, we use a fluidized bed experiment.

Fluidized beds show complex behavior, ranging from homogeneous expansion to situations where instabilities are propagated through the fluidized bed, for example in the case of plug flow with particle rain. The fluidization regime, i.e. the observed bed behavior, will determine the behavior of particles as well, which consequently determines the mechanism and rate of degradation. There has been extensive research into fluidized beds and how their behavior relates to particle and fluid properties (either gas or liquid phase). Van Wijk et al. (2016) studied the propagation of instabilities in vertical transport system in the context of deep sea mining by emulating the VTS with a fluidized bed setup. It was found that the wide range of fluidization regimes as reported in literature on gas-solid fluidization (see for instance Geldart (1973)) is less pronounced or even absent in water-solid systems with large or dense particles like ours. Van Wijk et al. (2016) reports on fluidization experiments with glass beads ($\rho_s \approx 2500\ \mathrm{kg/m^3}$) in water, which is very similar to the system of polymetallic nodules in water we use in this study, both in size and particle properties. The dominant fluidization regimes as found by Van Wijk et al. (2016) were plug flow with particle rain at high volume fractions of solids, developing into more homogeneous fluidization with frequent particle collision when the volume fraction of solids was decreased (by increasing the water velocity). These flow regimes hardly differ from real transport conditions.

The setup in this study is designed to match the traveled distance of the nodules in a VTS, assuming that the relative particle velocities are dominant in the attrition process rather than the mixture bulk velocity. The Stokes number of a particle in vertical pipe flow describes it's inertia relative to fluctuations in the flow field. Particles with a high Stokes number ($St \gg 1$) detach from the flow, while particles with low Stokes number ($St \ll 1$) number follow the flow well. The Stokes

number of a nodule in vertical flow is the ratio between the particle reaction time $t_p$ and the time scale of the surrounding flow $t_f$.

$$St = \frac{t_p}{t_f} \tag{2}$$

The time scale of the environment we chose to be the mixture velocity $v_m$ over the pipe diameter $D$, representative for the largest eddies possible in a pipe cross section.

$$t_f = D/v_m \tag{3}$$

The particle reaction time $t_p$ is defined as 63% of the time needed to reach terminal settling velocity, starting from a stationary position (Crowe et al., 2012). This is calculated by solving the equation of motion of a particle with hydrodynamic drag, buoyancy and gravity forces. An analytical solutions to this is available in Van Wijk et al. (2019). A 35 mm nodule in a 0.3 m pipe, further using the same conditions as the jumper hose, has a Stokes number of $St = 1.87$. This tells us that the inertia of the particle is large compared to the hydrodynamic forces acting on it. Combined with the large size relative to the pipe diameter, collisions will be frequent when particles of different sizes attempt to pass each other. These collisions are much more common (and more intense) than in case of smaller particles with low Stokes numbers, as these tend to avoid each other by following the fluid. Therefore the third experiment is designed such that the particle Stokes number is representative for flow in the full scale VTS.

### 2.2. Abrasive wear of individual nodules

When two bodies are in sliding contact, material is removed on their interface due to abrasive wear. The real contact area between the bodies is dominated by the deformation of their asperities. Archard (1953) assumes pure plastic deformation of the bodies which directly relates to the normal load, resulting in a material volumetric loss $V$ that linearly relates to the normal load $F_n$ on the bodies and the sliding distance $s$:

$$V = k \cdot F_n \cdot s \tag{4}$$

The assumption of pure plastic deformation is not perfectly valid for brittle materials like polymetallic nodules, but it is not known where the limits are. To test Archard's equation an experiment is needed where the mass loss of a nodule is measured and the sliding distance is varied as independent parameter. Another experimental parameter is the normal force, which is varied by testing nodules of various sizes and mass.

The test setup consists of a transparent PVC pipe with a diameter of 150 mm and a length of 1.5 m and with blind flanges at both ends, see Fig. 2 and Fig. 3. The pipe is filled with water and a single nodule and by tilting back and forth, the nodule slides along the bottom of the pipe. The experiment continues until the nodule has traveled the desired distance. The transparent pipe enables camera recordings of the nodule motion which will be used for analysis of the normal force acting on the nodule. An electrical motor, connected via a crankshaft mechanism to the pipe, governs the tilting motion. A high speed camera (DEWESoft DS-CAM-600) is rigidly fixed to the tilting pipe such that the camera footage is fixed relative to the movement of the pipe. Fig. 4 shows a snapshot of the sliding motion of a single nodule during one of the experiments. Each end of the pipe is closed of with a blind flange, which is covered with soft rubber to avoid high impact forces and consequently impact degradation. A step counter keeps track of the total number of cycles and the pipe angle is measure continuously with a high precision potentiometer. All measured signals, including camera footage, are synchronized and logged using a DEWEsoft SiriusI data logging system.

Each test is conducted with a fresh, unworn nodule. In the test setup the sliding velocity of the nodules will not be constant due to acceleration and deceleration of the nodule. By testing nodules of different sizes (and masses) at constant tilting speed (determined by the rotational speed of the motor), different (average) nodule velocities are obtained. In this way the setup allows for testing whether the wear rate is independent on the velocity. If a non-linear relationship is found between the wear rate and the sliding distance the hypothesis is falsified. A linear relationship between the worn volume and sliding distance confirms the validity of Archard's relationship for pure abrasion of polymetallic nodules. The typical mass loss of a nodule during an experiment will be in the order of grams, which is too little to obtain a PSD of the degraded material with standard sieves. Therefore this experiment cannot give precise insight in the fraction of fines smaller than 63 μm.

In order to arrive at the specific wear rate $k$, the following procedure was followed. Eq. (4) relates to the worn volume $V$, which is related to the mass loss during an experiment. The mass loss $\Delta m = m_0 - m_1$ is determined from the difference between pre- and post-experiment mass of the nodule (measured with a Mettler Toledo scale with $1 \cdot 10^{-4}$ gram precision). Additionally the wear is a function of the normal force acting on the particle, changing as a function of the pipe angle $\theta$. $F_n$ is calculated as:

$$F_n = m_0 \cdot \left(1 - \frac{\rho_f}{\rho_s}\right) \cdot g \cdot \cos\theta \tag{5}$$

Where $m_0$ is the initial nodule mass, $\rho_f$ the water density and $\rho_s$ the density of a polymetallic nodule. Note that the normal force is calculated using the initial mass and does not account for the mass loss. Doing any better than this is difficult as the mass loss rate is unknown and it will be shown later that the maximum mass loss measured was only 1.8%. In retrospect, this will only produce a small insignificant error compared to the large variation in the nodule mechanical properties. The inclination angle $\theta$ of the nodule is determined from the pipe's inclination angle and the camera footage. Using video tracking software the position of the nodule relative to the pipe is known as function of time, together with the pipe's inclination angle.

The sliding distance $s$ is calculated from the pipe length and the amount of measured tilting motions. The nodule density was measured from ten nodules with an average of 2497 kg/m$^3$ with a standard deviation of 336.9 kg/m$^3$. Together with the measured mass loss and the normal force the specific wear rate $k$ is calculated using:

$$k = \frac{\Delta m}{F_n \cdot \rho_s \cdot s} \tag{6}$$

### 2.3. Particle-particle contribution in sliding bed wear

The single nodule tests described in Section 2.2 give insight in the principles governing wear, but they are unrealistic compared to actual horizontal slurries where nodules are transported as a sliding bed and

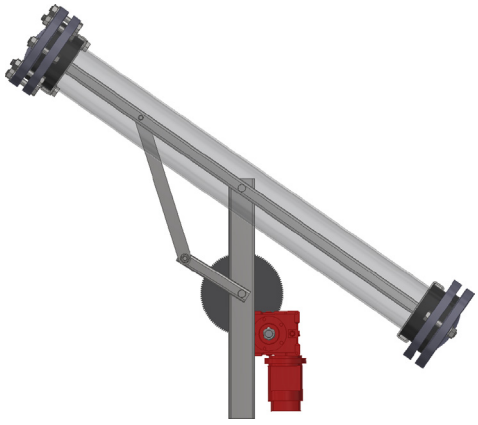

**Fig. 2.** Front view of the tiling pipe setup.

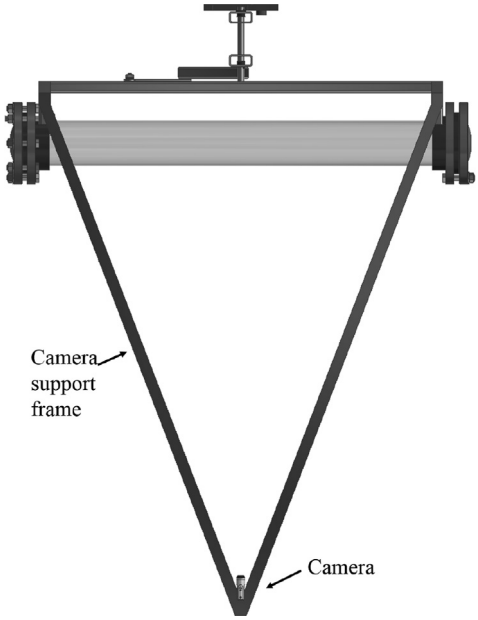


**Fig. 3.** Top view of the tilting pipe setup, showing the high speed camera following the tilting pipe motion.

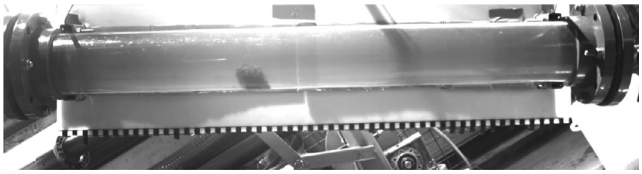

**Fig. 4.** A polymetallic nodule sliding from left to right in the tilting pipe setup.

by saltation. With these transport modes the wear is expected to be significantly higher due to a higher normal force on particles on the pipe wall and a large amount of particle-particle contact. On top of this the single nodule experiments do not give insight in the amount of fines ($d < 63\ \mu m$), because the mass of the degraded material was too low to analyse the distribution of the abraded material. The next experiment will use the same tilting pipe setup, but with a batch of nodules. This is the closest to simulating the sliding bed flow encountered in the jumper hose of a VTS.

We discussed that the conditions of the setup should be similar to the full scale jumper hose, using the Rouse number ($P > 2.5$). In a jumper hose the bed slides because a shear flow acts on top of the bed layer, effectively pulling the bed forward, and the Rouse number is determined by the relative velocity between the bed and the flow. In the experiment the bed slides due to gravity while the flowrate above the bed is approximately zero. The relative velocity of the bed was observed to be approximately 0.7 m/s maximum, resulting in $P \approx 5$, which is sufficient to emulate saltating flow. Our observations of the experiment confirm some saltating and rolling behavior of the nodules.

**Fig. 6.** A bed of nodules placed in the tilting pipe setup.

The PSD of polymetallic nodules is made to have a balanced representation of millimeter to tens of millimeter scale nodules, which is expected to resemble prototype conditions. In Fig. 5 a snapshot during one of the batch experiments, seen from the high speed camera, is shown.

The influence of abrasive wear is determined by the comparison of the initial distribution and the distribution after the experiment. Figs. 6–8 give an impression of the nodule batch and the residual fines created during an experiment.

After testing, all material from the pipe is collected by flushing the setup with tap water. To allow the nodules to be used again for a follow-up test, the largest fractions ($d > 2.8$ mm) were sieved wet and their weight later corrected for the water content. All remaining fractions were collected and allowed to settle until separation from the water was achieved. After settling, the clean water was carefully removed from the concentrate by means of a small venturi pump. The concentrate was dried to evaporate any remaining water and the dry material was sieved to produce a PSD.

### 2.4. Particle-particle collisions in vertical flow

The test setup used to study the nodule wear process in the vertical riser of a VTS is given in Fig. 9. A vertical 5 m long pipe with a diameter of 150 mm is placed between two 3 mm screens. Water flows between the nodules with a mean velocity of 0.8 m/s, which is just above the fluidization velocity allowing the nodules to slowly travel upwards. Once all nodules reach the top screen the pump is turned off and the nodules are allowed to settle, a 45 s cycle. This cycle is repeated until a

**Fig. 5.** Sliding of the batch of nodule inside the experimental setup.

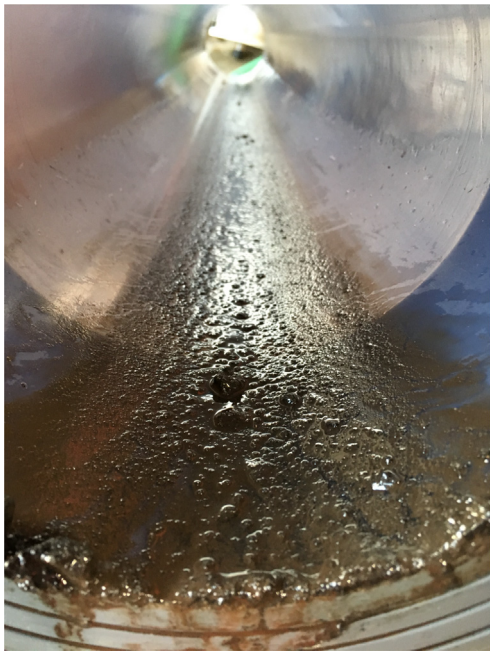

**Fig. 7.** Remaining fines residue after testing a bed of nodules in the tilting pipe.

**Fig. 8.** Samples of various size classes.

desired traveling distance is achieved. The water with the degraded fines is able to pass through the screens and is circulated around the flow loop. Once the test was completed the water was pumped into a settling tank where the fines and large nodules are collected separately. In Section 2.1 we discussed how the Stokes number of the experiment should be of the same order as to the conditions in the VTS. These vertical flow experiments were conducted with $d = 45$ mm and $d = 65$ mm nodules, giving Stokes numbers of $St = 0.70$ and $St = 0.93$ respectively. These numbers are a bit smaller than the numbers on prototype scale ($St = 1.87$ for $d = 35$ mm nodules in a $D = 300$ mm riser), which means that the effect of particle inertia is slightly underestimated in our experiments (see Fig. 10).

Degradation during vertical hydraulic transport is governed to a large extent by the nodule hydrodynamics. Nodules are suspended in a turbulent pipe flow and they are primarily subjected to gravity, buoyancy and hydrodynamic drag forces in which both individual nodule properties and the nodule-water mixture bulk properties play a role. The combination of forces acting on the nodules results in the nodules having a relative velocity with respect to the surrounding fluid. The velocity difference, the slip velocity $v_{sl}$, is a function of nodule and bulk properties.

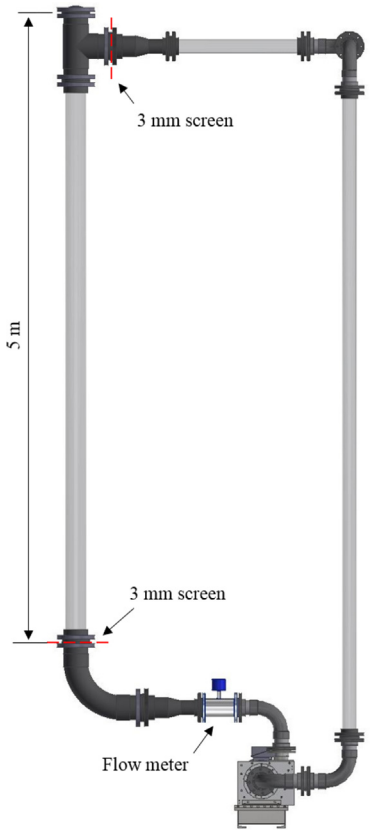


**Fig. 9.** A schematic overview of the vertical flow experiment.

The work of Richardson and Zaki (1954) gives a relation between the volume fraction of solids in a fluidized bed and the fluid velocity in the fluidization column:

$$v_{sl} = w_t \cdot 10^{-d/D} \cdot (1 - c_v)^n \tag{7}$$

In which $v_{sl}$ is the slip velocity or relative velocity of the nodules with respect to the mixture velocity, $w_t$ the terminal settling velocity of a single polymetallic nodule, $d$ the nodule diameter, $D$ the fluidization column internal diameter, $c_v$ the volume fraction of solids and $n$ an exponent. $n$ is a function of the particle Reynolds number $Re_p$.

The work of Richardson and Zaki (1954) has been extended for polydisperse mixtures by Mirza and Richardson (1979) and Lockett and Bassoon (1979). Successive work by among others Di Felice (1995), Di Felice (1999), Falk and D'Ortona (2002), Berres et al. (2005), Basson et al. (2009), Kramer et al. (2019) shows that the general framework of Eq. (7) has not changed. The major contribution of these authors is in further detailing of the exponent $n$, improving the insight in modeling polydispersity and the use of this model in the extreme case of the concentration approaching the packing limit (which is the case at the onset of fluidization and which is relevant in many industrial processes). In our experiments we operate far above the onset of fluidization which leads us to conclude that the model of Eq. (7) is valid.

The exponent $n$ as initially described by (Richardson and Zaki, 1954) lies in the range $2.39 \leqslant n \leqslant 4.65$. The work of Garside and Al Dibouni (1977), Rowe (1987) and Di Felice (1999) has increased the understanding of the actual physics underlying $n$ and it has shown that for different situations the upper limit is subject to change, but as Kramer et al. (2019) shows the lower limit of $n \approx 2.4$ remains unchanged. In our experiments the inert nodules, having large particle Reynolds numbers, are the dominant contributors to nodule degradation. This leads to $n = 2.4$ in our experiments.

The individual nodule settling velocities $w_t$ determines the maximum slip velocity, while the term related to the volume fraction of

**Fig. 10.** Polymetallic nodules traveling in the vertical flow experiment.

solids corrects this velocity for the changed conditions in the presence of other suspended particles. The terminal settling velocity is a function of the particle density $\rho_s$, the fluid density $\rho_f$, the particle diameter $d$, the gravitational constant $g$ and the drag coefficient $C_D$:

$$w_t = \sqrt{\frac{4 \cdot g \cdot d \cdot (\rho_s - \rho_f)}{3 \cdot C_D \cdot \rho_f}} \tag{8}$$

The drag coefficient of a perfect sphere is very well documented with a good overview given in Cheng (2009). Similar models are available for non-spherical particles, see for instance Tran-Cong et al. (2004) or Zastawny et al. (2012), which are especially useful for simulation purposes of small quantities of particles. Direct calculation of $w_t$ of irregularly shaped particles is a more practical approach for engineering purposes. Ferguson and Church (2004) have combined different empirical models and experimental data into a single formula for the calculation of $w_t$, valid for all particle Reynolds numbers.

Van Wijk et al. (2016) uses the combination of an empirical model for $w_t$ and Eq. (7) with the exponent $n$ according to Garside and Al Dibouni (1977) to model the slip velocity of polymetallic nodules during vertical hydraulic transport. Their experimental work on large spherical and non-spherical particles has shown that fluidization experiments combined with the models as described in this paper capture the dominant hydrodynamic features of nodule transport.

In the case of fluidization with a single nodule, the nodule will be kept in steady position when water flows with $v_f = w_t$ and consequently there is no transport. This is only valid for a single particle or a very dilute suspension. During transport conditions in the VTS, the nodules will be transported at a velocity $v_s = v_m - v_{sl}$. Where $v_m = v_s \cdot c_v + v_f \cdot (1 - c_v)$ is the mixture velocity. Particle-particle interactions are dominated by their relative velocities, so a fluidization experiment can be used to study nodule degradation by particle-particle interactions.

The fluidized bed experiments consist of cyclic expansion (and associated return to the initial conditions) of a packed bed of polymetallic nodules. This is a transient process in which the nodules will first accelerate and then decelerate again, followed by hindered settling to their original position. The relative particle velocities in both the fluidization part and the hindered settling part are governed by Eq. (7), but the transient operation of the system results in relatively large forces on the particles when they meet the end of the test setup after their upward motion. The same holds for the return to the initial position of the solids, resulting in relatively large forces between the particles in between the motions. This will most likely cause additional fragmentation of the nodule surface. Results are therefore expected to show an overestimation of wear caused by chipping or attrition.

The main degradation mechanisms expected in vertical segments of the VTS are particle-wall abrasion and particle-particle chipping and attrition. The velocity difference between the wall and nodules in the real VTS are in the order of the mixture velocity (~4 m/s) and the velocity difference between the particles is in the order of the hindered settling velocity of a particle (~0.5 m/s). In the experiment the velocity difference between the nodules and the wall is lower than on prototype scale while the relative velocities between the nodules are similar. The experiments therefore have a bias towards chipping and attrition and will underestimate the abrasion. Due to additional impacts at the ends of the test setup and due to the bias towards particle-particle interaction, the experiments are expected to give a conservative estimate of the production of debris due to attrition and chipping.

After a test, the fluidization column is emptied and the coarse material is sieved wet. A relatively large amount of clay was found in the fines of the slurry. This is clay from tiny pockets on the nodule surface and clay from between the nodule layered internal structure. The amount of clay was much more than encountered during the single nodule and batch nodule sliding tests and sufficient clay material was present to adhere to the degraded nodule particles when letting the nodule samples dry for sieving. During initial sieving it was observed that the nodule fines were covered with clay, which influenced the sieve analysis. This was concluded by observing the color of the samples, beige being clay and black being nodules, together with microscope observations. To avoid clay adhering to the nodule particles, immediately after an experiment the entire mixture was passed through a set of wet sieves with the smallest sieve being 40 μm, allowing all clay to pass through. However the sub 40 μm slurry still contains an unknown amount of nodule particles. To separate the clay from the nodule particles the remaining sub 40 μm slurry was left to settle for a few hours until only a black sedimentation layer formed. The water was still beige colored and would only settle after ~24 h. Thus by separating the water (with suspended clay) after several hours a good separation between sub 40 μm nodule particles and clay was achieved. This method was confirmed to be successful with microscope observations of the dried samples. The nodule sample showed mainly black nodule particles which are absent in the beige clay sample.

## 3. Results

### 3.1. Abrasive wear of individual nodules

A total of 18 tests were completed with single nodules with masses varying between 289.8 and 629.4 grams and sliding distances varying between 210 and 900 meters. For a typical experiment the mass lost from the nodule is in the order of a few grams. An overview of the conducted experiments can be seen in Table 1.

In Fig. 11 $\Delta m/(F_n \rho_s)$ is given as a function of the sliding distance for

**Table 1**
The tests conducted in the single nodule tilting pipe setup. The travelled distance $s$, the sieve size class of the nodule, the initial nodule mass $m_0$ and the mass loss after completing the test $\Delta m$.

| Test | $s$ [m] | *Size* [mm] | $m_0$ [g] | $\Delta m$ [g] |
|---|---|---|---|---|
| 1 | 600 | 75–63 | 376.9 | 5.47 |
| 2 | 600 | 75–6 | 289.8 | 4.25 |
| 3 | 690 | 75–63 | 328.8 | 5.92 |
| 4 | 900 | 75–63 | 405.1 | 1.07 |
| 5 | 300 | 75–63 | 345.6 | 1.95 |
| 6 | 300 | 75–63 | 432.1 | 2.40 |
| 7 | 375 | 75–63 | 410.8 | 4.26 |
| 8 | 300 | 75–63 | 383.5 | 5.76 |
| 9 | 300 | 75–63 | 364.9 | 4.73 |
| 10 | 225 | 63–45 | 287.6 | 0.20 |
| 11 | 210 | 80–75 | 629.4 | 3.61 |
| 12 | 210 | 80–75 | 431.5 | 1.76 |
| 13 | 210 | 80–75 | 504.1 | 2.30 |
| 14 | 375 | 80–75 | 502.5 | 4.69 |
| 15 | 510 | 80–75 | 461.0 | 6.15 |
| 16 | 450 | 80–75 | 384.6 | 3.36 |
| 17 | 450 | 75–63 | 344.0 | 4.28 |
| 18 | 690 | 75–63 | 309.7 | 3.86 |

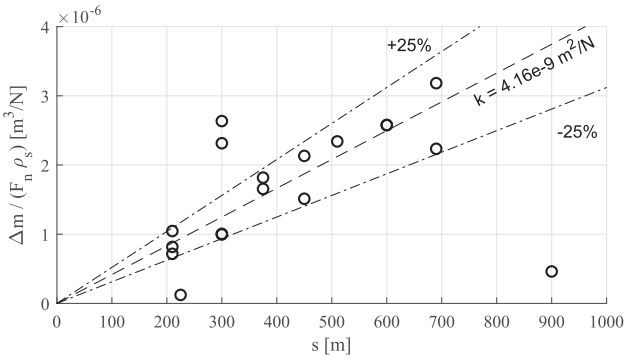


**Fig. 11.** The ratio of the mass loss over the normal force and the particle density, plotted as function of the sliding distance. The average corresponds with $k = 4.16{\cdot}10^{-9}$ m$^2$/N and most data points fall within a +25% to −25% range. The data points are gathered from nodules with various masses ranging between 289.8 and 629.4 grams.

each experiment and shows a linear relationship between the worn mass and sliding distance. This supports the validity of Archard's equation. The average Archard $k$ factor from these test was $k = 4.16{\cdot}10^{-9}$ m$^2$/N and is shown in Fig. 11 together with a +25% to −25% accuracy interval. Most data points fall within the 25% accuracy range. In case of four experiments the results fall far from the average and two tests show very little wear. This could be because the local hardness of the contact area was very high and the nodule did not shift position to another contact area during the experiment. However this explanation is speculative and could be confirmed by doing hardness tests on different parts of a nodule.

### 3.2. Particle-particle contribution in sliding bed wear

No Archard $k$ factor is calculated from these tests, since this would be an incorrect implementation of Archard's equation, because wear is not solely attributed to abrasion. Instead the particle size distribution is studied before and after the experiment. The same batch was tested twice over a distance of 4500 m, giving an accumulative traveled distance of 9000 m. The comparison between the starting PSD, the PSD after 4500 m and the PSD after 9000 m is shown in Fig. 12. Note that the vertical axis of the bar graph is logarithmic to visualize the development of the smaller fractions. The authors chose to display the results in a bar chart, in addition to the conventional cumulative distribution PSD, to better visualize the accumulation of material in the range of 500 μm to 125 μm (as explained below).

Fig. 12 shows that large fractions (>3.55 mm) decrease with each test and small fractions increase. This simply means that mass is transferred from the large fractions to the small fractions. An interesting observation is the accumulation of material in the range of 500 μm to 125 μm. If all particle sizes would keep degrading at the same rate then eventually all material will accumulate in the smallest classes (<38 μm), which is clearly not the case. This strongly suggests that the wear rate of material smaller than 500 μm is very low and their mass is no longer transferred to the smallest fractions by means of degradation. This is caused by the small particles becoming suspended in the fluid, resulting in less contact with other particles and the pipe wall and consequently less degradation.

Any particles smaller than 63 μm are considered as irrecoverable for dewatering of the polymetallic nodules. The mass fraction of irrecoverables is 0.36 wt% and 0.81 wt% for a sliding distance of 4500 m and 9000 m meters respectively.

### 3.3. Particle-particle collisions in vertical flow

Figs. 13 and 14 shows the results of the vertical flow fluidization tests. Fig. 13 shows a batch with nodules sized between 45–31.5 mm which underwent three tests with an accumulative traveled distance of 470 m, 1970 m and 4430 m. The lower graph shows the result of one test conducted with 63–45 mm nodules for a traveled distance of 1500 m to test the effect of particle size. The result of these tests show a similar trend as the sliding bed test (Fig. 12) in the sense that material accumulates in the range of 500 μm to 125 μm, because the particles are suspended by the water and their wear rate is reduced drastically.

Comparing the fluidization test results to the sliding bed experiments in Fig. 12, can only be done by comparing particles smaller than 1.00 mm, since the initial starting batch of the sliding bed experiment contained only particles larger than 1.00 mm, thus any a particle smaller than 1.00 mm is due to degradation. When comparing Figs. 12 and 13 for a traveled distance of 4500 m and 4430 m respectively, it is obvious that the fraction of degraded material smaller than 1.00 mm is lower for the vertical flow experiments than the sliding bed experiment (20.2 wt% and 10.4 wt% respectively <1.00 mm). The fraction of fines ($d$ < 63 μm) for the same tests is 0.36 wt% in the sliding bed test and 1.85wt% in the fluidization test. This is contradictory, because the fluidization test shows less wear over the entire PSD. This probably gives an indication of the accuracy of the method for collecting the fines. The weight of these fraction are sometimes smaller than one gram, with the total PSD mass being kilograms. A small mistake while sieving, like a spillage, will result in a large deviation. Nonetheless if we consider the highest measured fines fraction of 1.85 wt% it is still very low.

Fig. 14 shows the resulting PSD from a fluidization test with nodules starting in the 63–45 mm size class. After a traveled distance of 1500 m, 9.9 wt% degraded to a size smaller than 1.00 mm. This is already more compared to the 45–31.5 mm test after a traveling distance of 1970 m. This can well be because of the larger particle diameter. The vertical pipe in the test setup has an internal diameter of 150 mm, thus two or three 63–45 mm sized particles can barely fit within the pipe's diameter. The amount of fines was 0.42 wt% for the 63–45 mm test ($s$ = 1500 m) and 1.4 wt% for the 45–31.5 mm test ($s$ = 1970 m). However as already stated before, some inaccuracies are possible in measuring the fines so comparing these two is difficult. Nonetheless the fines fraction is in the same order and very small in magnitude.

## 4. Discussion

By testing small samples of polymetallic nodules we were able to provide insight in the magnitudes of nodule degradation due to pure abrasion and particle-particle interaction. All parameters were

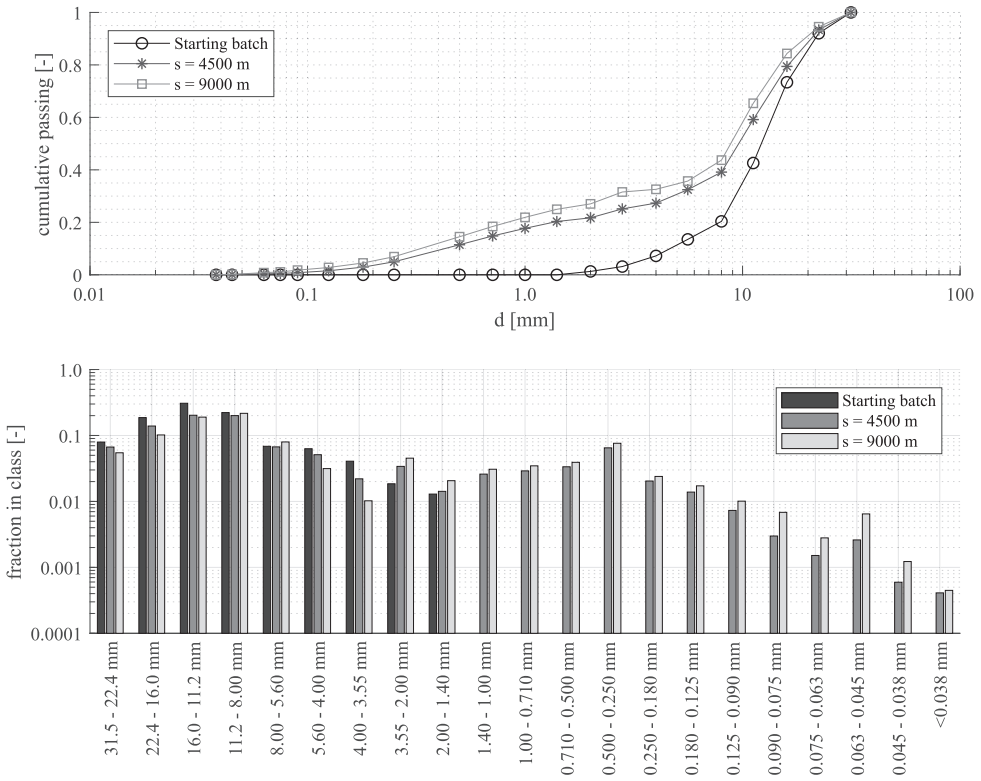


**Fig. 12.** The initial batch PSD and the remaining PSD after a sling distance of 4500 m and 9000 m, displayed in PSD (top) and bar plot (bottom).

measured with accurate instruments, however the overall accuracy of the results is dominated by large statistical deviation in nodule physical properties. This is visualized well in Fig. 11 (the single nodule sliding experiments). The calculated specific wear rate $k$ has a large deviation which can be attributed mainly to the difference in the strength and density of each individual nodule. The results could have been made more accurate by measuring the density of each specimen individually and use this density to calculate the normal force, instead of using an

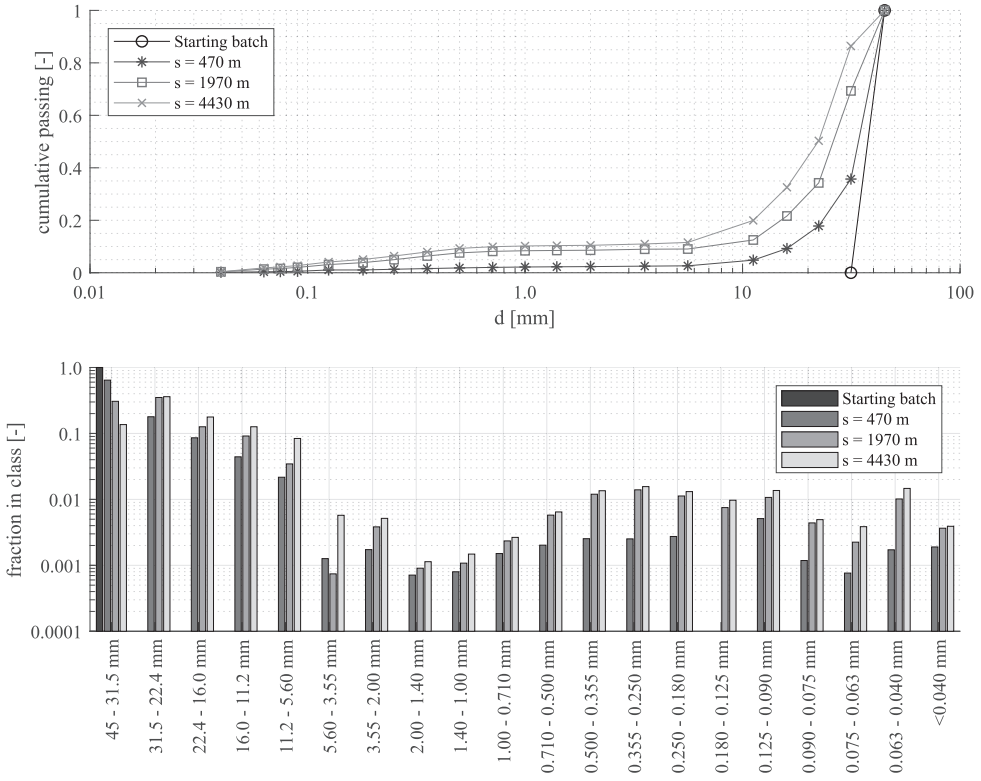


**Fig. 13.** The change of particle size in the vertical fluidization experiment starting with nodules of the 45–31.5 mm class and three consecutive experiments, displayed in PSD (top) and bar plot (bottom).

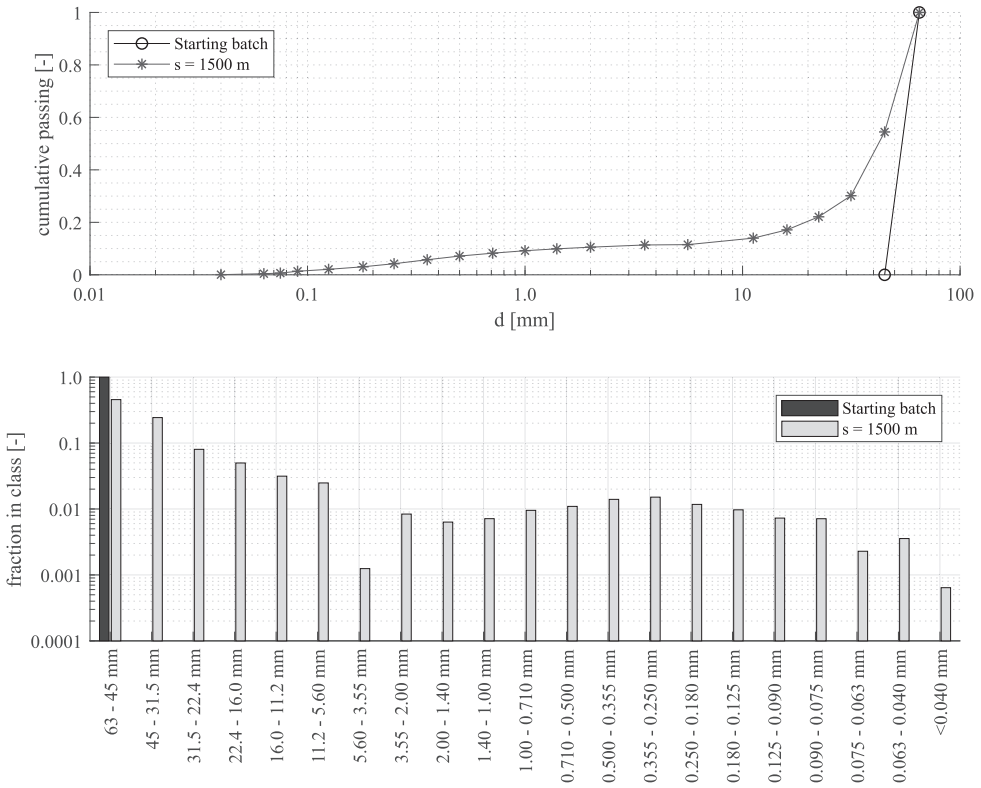


**Fig. 14.** The change of particle size in the vertical fluidization experiment starting with nodules of the 65–45 mm class, displayed in PSD (top) and bar plot (bottom).

average nodule density.

The accuracy of the sliding batch and vertical flow experiments are mainly dominated by human error. Small spillages of samples during sieving can have large effects on determining the mass of the smallest fractions (<75 μm in the sieves used), which were typically smaller than one gram. It is important to be aware of this when evaluating the quantity of the smallest classes found in Figs. 12–14. Even though the magnitude could be inaccurate, comparing the different size classes is still useful to discover various trends, as done in Section 3, e.g. resulting in conclusions and observations about the accumulation of material in the range of 500 μm to 125 μm.

The three experiments show nodule degradation under three different degradation modes. The single nodule sliding experiment in the tilting pipe shows degradation as pure abrasion, since the degradation force is parallel to the pipe wall. This experiment shows the lowest degradation rate of the three experiments, because this experiment does not include degradation by particle-particle collisions, unlike the other two experiments.

The titling pipe batch experiment degradation process includes, on top of particle-wall abrasion, particle-particle abrasion and attrition as particles saltate and roll over each other. This increases the amount of collisions, as nodules are practically in constant contact with each other, with a higher degradation rate as a result. The amount of particle-particle and particle-wall collisions in these tests is highest of all three experiments, which is reflected in the highest measured degradation of the three experiments.

Finally the vertical flow experiment shows combined abrasion and attrition through particle-wall and particle-particle collisions. Visual observations show that the amount of collisions is less frequent than the tilting pipe saltating degradation process. This is simply due to the nature of the fluidization experiment where particles are spaced farther apart than in a saltating flow. During the vertical experiment collision with the wall is not a continues sliding process, the nodules rather sporadically slide and bounce of the wall. This bouncing most likely causes additional degradation by chipping and attrition. In case of pure abrasion we expect the degradation due to wall collisions to be less than the degradation found in the single nodule titling pipe test, since sliding is not continues and the gravity vector is parallel to the pipe wall in the case of fluidization. The overall degradation is measured to be significantly higher in the vertical flow experiment than in the single sliding experiment. Therefore a logical conclusion is that degradation in the vertical flow experiment is dominated by attrition and chipping due to particle-wall and particle-particle collisions and there is very little abrasion.

The degradation as found in this article is specific to the nodule samples used in this study and specific to the VTS design we considered. With a different internal pipe diameter, nodules size or density, the measured degradation rates are still representative as long as the transport modes do not change (similar Rouse and Stokes numbers). However the CCZ is an area half the size of the United States, therefore nodule strength is likely to vary with location and consequently degradation rates are likely to show variation. The degradation mechanisms however have a more general validity and these experiments can easily be repeated when nodules with different strengths and characteristics are encountered. These tests can also be used to investigate degradation of other brittle minerals for that matter, as long as the experiments remain representative for the transport mode of the hydraulic transport system.

## 5. Conclusions and recommendations

The single nodule sliding experiments show that mass loss due to abrasion increases linearly with the sliding distance and a specific wear rate $k$ could be determined within 25% accuracy based on the model of Archard (1953). The average wear rate under atmospheric conditions in fresh water was found to be $k = 4.16 \cdot 10^{-9}$ m$^2$/N, based on sliding distances varying between $200 < s < 700$ m. A few outliers were found for which no explanation can be found other than variation of nodule properties.

The sliding batch experiments were expected to yield a conservative

estimate of the amount of fines produced after multiple kilometers of transport. We observed abrasion of nodules in the classes with $d > 3.55$ mm (material loss from the class after $s = 4500$ m and $s = 9000$ m of sliding) and an increase in mass in the smaller size classes. Most notably, the tests show accumulation of material in the $d = 0.500 - 0.250$ mm size class, pointing at very low wear rates of the smaller material. The small particles could be suspended in the water or be entrained in the pores of the matrix of larger nodules, thus being protected from abrasion. After $s = 9000$ m of sliding, the amount of fines $d < 0.063$ mm is 0.81 wt%.

While we expected the sliding batch to yield a conservative estimate of fines production, larger amounts of fines were measured during the fluidization experiment. The combination of particle-particle interaction and collision of nodules with the ends and side walls resulted in accumulation of material in the $d = 0.500 - 0.250$ mm class, just as was found for the sliding batch experiments. This occurred for virgin nodules with $31.5 < d < 45$ mm as well as for $45 < d < 65$ mm. The fluidization tests with $31.5 < d < 45$ mm virgin nodules resulted in 20.2 wt% of material in the size class $d < 1.00$ mm. The total amount of fines produced during fluidization of the polymetallic nodules with virgin size $31.5 < d < 45$ mm after $s = 4430$ m is 1.85 wt%. Determination of the amounts of material in the smallest size classes is sensitive to human errors due to the very small quantities involved, but at least the order of magnitude is indicative for real vertical transport processes.

This work aims at quantification of degradation of polymetallic nodules during vertical transport due to particle-wall and particle-particle interaction. It builds on earlier research work on impact fragmentation. We conducted three experiments focussed on the production of finer material, since the finer material fractions are considered hard to recover in the processing of the ore and are considered to be potentially harmful when returned into the ocean. When considering the degradation of all particle sizes, the single nodule tilting tube test shows very low degradation. Degradation measured in this experiment provides a lower boundary to the fines production, since only pure abrasion is taken into account. It is therefore too low as an estimate for the entire system. The sliding bed experiment with a batch of nodules shows very high degradation rates, representative for the lazy-wave jumper hose and horizontal saltating flows. The degradation rate measured in the fluidization experiment is the most realistic representation of the vertical transport in the VTS. Together, these three experiments provide a good bandwidth of degradation rates which allows for the analysis of different scenarios in engineering practice.

For future work it remains to combine the current results and the earlier work on impact fragmentation into a single framework for assessment of degradation of polymetallic nodules during vertical transport. This framework should be a combination of modeling and standardized experiments. The fluidization experiment would be the best option to include in this framework.

## CRediT authorship contribution statement

**E. de Hoog:** Methodology, Validation, Formal analysis, Investigation, Writing - original draft. **J.M. van Wijk:** Conceptualization, Methodology, Writing - original draft, Resources, Supervision. **J.T.M. Wijnands:** Formal analysis, Investigation, Writing - original draft, Visualization. **A.M. Talmon:** Writing - review & editing, Supervision.

## Declaration of Competing Interest

The authors declare that they have no known competing financial interests or personal relationships that could have appeared to influence the work reported in this paper.

## Acknowledgments

The research in this article is funded by the EU H2020 Research and Innovation programme under Grant Agreement no. 688975 and by Royal IHC, The Netherlands. The authors thank GSR NV for providing the polymetallic nodules. We thank Jazzie Hoebe from IHC MTI for the design and construction of the tilting pipe test setup and the related figures in this article.

## References

Archard, J., 1953. Contact and rubbing of flat surfaces. Appl. Phys. 24 (3), 981–988.
Basson, D.K., Berres, S., Bürger, R., 2009. On models of polydisperse sedimentation with particle-size-specific hindered-settling factors. Appl. Math. Model. 33, 1815–1835.
Berres, S., Bürger, R., Tory, E.M., 2005. Applications of polydisperse sedimentation models. Chem. Eng. J. 111, 105–117.
Cheng, N., 2009. Comparison of formulas for drag coefficient and settling velocity of spherical particles. Powder Technol. 189, 395–398.
Crowe, C.T., Schwartzkopf, J.D., Sommerfled, M., Yutaka, T., 2012. Multiphase flows with droplets and particles, 2nd Edition. CRC Press, Boca Raton, FL.
De Hoog, E., In 't Veld, J., Van Wijk, J., Talmon, A., 2017. An experimental study into flow assurance of coarse inclined slurries. In: 18th International Conference on the Transport and Sedimentation of Solid Particles, 11-15 September, Prague, Czech Republic.
Di Felice, R., 1995. Hydrodynamics of liquid fluidisation. Chem. Eng. Sci. 50 (8), 1213–1245.
Di Felice, R., 1999. The sedimentation velocity of dilute suspensions of nearly monosized spheres. Int. J. Multiphase Flow 25, 559–574.
Dreiseitl, I., 2017. About geotechnical properties of the deep seabed polymetallic nodules. In: 18th International Conference on the Transport and Sedimentation of Solid Particles, 11-15 September, Prague, Czech Republic.
Falk, V., D'Ortona, H., 2002. A polydisperse sedimentation and polydisperse packing model. Powder Technol. 128, 229–235.
Ferguson, R.I., Church, M., 2004. A simple universal equation for grain settling velocity. J. Sediment. Res. 74 (6), 933–937.
Garside, J., Al Dibouni, M.R., 1977. Velocity-voidage relationships for fluidization and sedimentation in solid liquid systems. second Eng. Chem. Process Des. Dev. 16, 206.
Geldart, D., 1973. Types of gas fluidization. Powder Technol. 7, 285–292.
Kramer, O., de Moel, P., Baars, E., van Vugt, W., Padding, J., van der Hoek, J., 2019. Improvement of the richardson-zaki liquid-solid fluidisation model on the basis of hydraulics. Powder Technol. 343, 465–478.
Lockett, M., Bassoon, K., 1979. Sedimentation of binary particle mixtures. Powder Technol. 24, 1–7.
Mirza, S., Richardson, J.F., 1979. Sedimentation of particles of two or more sizes. Chem. Eng. Sci. 34, 447–454.
Moore, M., King, F., 1980. Abrasive wear of brittle solids. Wear 60, 123–140.
Ravelet, F., Bakir, F., Khelladi, S., Rey, R., 2013. Experimental study of hydraulic transport of large particles in horizontal pipes. Exp. Thermal Fluid Sci. 45, 187–197.
Richardson, J., Zaki, W., 1954. Sedimentation and fluidisation: Part i. Trans. Inst. Chem. Eng. 32, S82–S100.
Rowe, P.N., 1987. A convenient empirical equation for estimation of the richardson and zaki exponent. Chem. Eng. Sci. 42 (11), 2795–2796.
Tran-Cong, S., Gay, M., Michaelides, E.E., 2004. Drag coefficients of irregularly shaped particles. Powder Technol. 139, 21–32.
Van Laarhoven, B., Maart 2010. Breakage of agglomerates. Ph.D. thesis, Delft University of Technology.
Van Wijk, J., 2016. Vertical hydraulic transport for deep sea mining, a study into flow assurance. Ph.D. thesis. Delft University of Technology.
Van Wijk, J., Haalboom, S., De Hoog, E., De Stigter, H., Smit, M., 2019. Impact fragmentation of polymetallic nodules under deep ocean pressure conditions. Miner. Eng. 134, 250–260.
Van Wijk, J., Talmon, A., Van Rhee, C., 2016. Stability of vertical hydraulic transport processes for deep ocean mining: An experimental study. Ocean Eng. 125, 203–213.
Vlasak, P., Chara, Z., Konfrst, J., Kysela, B., 2013. Experimental investigation of coarse-grained particles in pipes. In: 16th International Conference on the Transport and Sedimentation of Solid Particles, 18-20 September, Rostock, Germany, No. 60, pp. 3969–3992.
Wilson, K.C., Addie, G.R., Sellgren, A., Clift, R., 2006. Slurry Transport using Centrifugal Pumps, 3rd Edition. Springer, US.
Worster, R., Denny, D., 1955. Hydraulic transport of solid material in pipes. Proc. Inst. Mech. Eng. 169 (1), 563–586.
Zastawny, M., Mallouppas, G., Zhao, F., Van Wachem, B., 2012. Derivation of drag and lift force and torque coefficients for non-spherical particles in flows. Int. J. Multiphase Flow 39, 227–239.